Article ID: 1000-7032(2022)12-1871-21

A Tutorial Review on the Nonradiative Energy Transfer Rates between Lanthanide Ions

Albano N Carneiro Neto[1], Renaldo T Moura Jr[2,3], Jorge A A Coelho[4,5], Mauro E Silva-Junior[4,5], Janderson L Costa[4,5], Oscar L Malta[4*], Ricardo L Longo[4*]

(1. *Physics Department and CICECO-Aveiro Institute of Materials, University of Aveiro, Aveiro, Portugal*, 3810-193;
2. *Department of Chemistry, Southern Methodist University, Dallas, United States*, 75275-0314;
3. *Department of Chemistry and Physics, Federal University of Paraíba, Areia, Brazil*, 58397-000 (*permanent address*);
4. *Departamento de Química Fundamental, Universidade Federal de Pernambuco, Recife, Brazil*, 50740-560;
5. *Programa de Pós-Graduação em Ciência de Materiais, Universidade Federal de Pernambuco, Recife, Brazil*, 50670-901)
* *Corresponding Authors, E-mail: oscar. malta@ufpe. br; ricardo. longo@ufpe. br*

Abstract: In this tutorial review, we present nonradiative energy transfer(ET) rates between lanthanides in a rearranged form. We emphasize the nature of the contributions which are different from those developed by Förster and Dexter theories because of the unique properties of the lanthanide ions. The expressions discussed here were based on Kushida's approach (electric multipolar mechanisms: dipole-dipole ($W_{d\text{-}d}$), dipole-quadrupole ($W_{d\text{-}q}$), and quadrupole-quadrupole ($W_{q\text{-}q}$)) within the Judd-Ofelt framework for 4f-4f transitions. Notice that these mechanisms were extended to include the exchange (W_{ex}) and magnetic dipole-magnetic dipole mechanisms ($W_{md\text{-}md}$), and were improved to include shielding effects as well as an analytical expression for the *F*-factor (density of states in Fermi's golden rule). Similar to the original approach of Kushida, only the Forced Electric Dipole(FED) contributions to the Judd-Ofelt intensity parameters should be considered. A detailed discussion of selection rules and matrix elements calculations for the magnetic dipole-magnetic dipole interaction is presented. In addition, step-by-step examples of Tb(Ⅲ)-Eu(Ⅲ) and Yb(Ⅲ)-Er(Ⅲ) energy transfer rates calculations are provided, with extensive Supporting Information, including scripts for calculations.

Key words: nonradiative energy transfer; lanthanides; theoretical calculations; *Ln-Ln* energy transfer rates; selection rules

CLC number: O482.31 **Document code**: A **DOI**: 10.37188/CJL.EN20220007

镧系离子间无辐射能量传递速率的教程综述

Albano N Carneiro Neto[1], Renaldo T Moura Jr[2,3], Jorge A A Coelho[4,5], Mauro E Silva-Junior[4,5], Janderson L Costa[4,5], Oscar L Malta[4*], Ricardo L Longo[4*]

(1. 阿威罗大学 物理系和 CICECO-阿威罗材料研究所, 阿威罗, 葡萄牙, 3810-193;
2. 南卫理公会大学 化学系, 达拉斯, 美国, 75275-0314; 3. 帕拉伊巴联邦大学 化学与物理系, 阿雷亚, 巴西, 58397-000;
4. 伯南布哥联邦大学 基础化学系, 累西腓, 巴西, 50740-560; 5. 伯南布哥联邦大学 材料科学研究生院, 累西腓, 巴西, 50670-901)

摘要: 在本教程综述中,我们重新阐述和表达了镧系离子间无辐射能量传递(ET)速率的理论形式,并且强调了考虑镧系离子本身特异性所引发的与 Förster 和 Dexter 理论不同之处。所给出的表达式遵循了 Judd-Ofelt 的 4f-4f 跃迁理论框架之下的 Kushida 方法,并计入了如下电多极机制:偶极-偶极($W_{d\text{-}d}$)、偶极-四极($W_{d\text{-}q}$)和四

收稿日期: 2022-05-20; **修订日期**: 2022-06-19

极-四极($W_{q\text{-}q}$)。更为重要的是,当前的机制也扩展包括了交换(W_{ex})和磁偶极子-磁偶极子($W_{md\text{-}md}$)作用,并经过改进进一步包含了屏蔽效应以及给出了 F 因子(费米黄金规则中的态密度)的解析表达式。与 Kushida 的原始方法类似,我们只考虑了强制电偶极子(FED)对 Judd-Ofelt 强度参数的贡献,并细节性地讨论了磁偶极-磁偶极相互作用的选择定则以及相关矩阵元的计算。此外,我们还以 Tb(Ⅲ)-Eu(Ⅲ)和 Yb(Ⅲ)-Er(Ⅲ)的能量传递速率计算为例,逐步展示了计算过程、主要的计算支撑信息以及所使用的计算脚本。

关 键 词:无辐射能量传递;镧系;理论计算;*Ln-Ln* 能量传递速率;选择定则

1 Introduction

Energy transfer(ET) processes are ubiquitous in nature and are essential to life[1-2]. Despite being difficult to visualize, these ET processes are always present in our everyday life and obey the laws of thermodynamics (for macroscopic systems). Many modern technologies are based on ET processes, for instance, those involving luminescence, where an excited sensitizer transfers energy to an activator that emits light (or electromagnetic radiation). Most results of these ET processes are visible and quantifiable, but their detailed understanding and description, at the microscopic level, requires quantum mechanics. As a result, at least two concepts are important, namely, (quantum) states and transitions between these states.

Photoluminescence involving lanthanide ions has some unique and remarkable features, which have been explored in many applications and new technologies, from biomedicine to engineering, and public health to public safety[3-7]. Energy transfer between lanthanide ions is particularly relevant to several processes such as long-range energy migration and energy upconversion. Resonances present in systems containing lanthanide ions of the same type, *e. g.*, Yb(Ⅲ), allow the energy to be efficiently transferred between these ions, which can migrate for long distances depending on their concentration and the host matrix[8-11]. On the other hand, a lanthanide ion with relatively large oscillator strength, *e. g.*, Yb(Ⅲ) and Nd(Ⅲ), can be employed as a sensitizer of another lanthanide ion, *e. g.*, Er(Ⅲ) and Tm(Ⅲ), called an activator, which can be excited by sequential energy transfer processes, followed by emission of photons with higher energy than those absorbed photons; hence energy upconversion[10,12-13]. In this context, energy transfer between lanthanide ions (*Ln-Ln* ET) plays a fundamental and essential role in several processes that are explored and exploited in applications and new technologies[14-16]. Therefore, the focus of this contribution will be the quantitative description of the *Ln-Ln* ET processes.

A common picture used for a general ET process employs two subsystems denoted as donor(D) and acceptor(A). Initially, the donor is prepared in an excited state, D^*, by absorbing energy(light, heat, and mechanical), which may be represented as $|i\rangle = |D^*A\rangle$. In other words, in the initial state, the energy absorbed by the system is localized at the donor subunit. Then, the system undergoes a transition to another state with the energy localized at the acceptor subsystem, represented as $|f\rangle = |DA^*\rangle$. This general description requires some clarification and specification of different categories of ET processes as well as additional phenomena accompanying these processes. For instance, energy transfer can induce or be caused by electron (or charge) transfer between the subsystems. These coupled processes are important and relevant for many biological systems and applications, but they will not be considered here. The ET processes of interest are uncoupled energy transfer processes in the sense that are not caused nor can induce electron transfer. This is an important distinction that is not always clear in the literature and has caused some confusion.

The transition mentioned above describes an ET process, represented by $|D^*A\rangle \rightarrow |DA^*\rangle$, can be pictured as a deexcitation of the donor and an excitation of the acceptor, which may or may not involve photon(s). When the deexcitation of D^* occurs by

photon emission (with energy $\hbar\omega=h\nu$), $|D^*\rangle \rightarrow |D\rangle + h\nu$, and the emitted photon is absorbed by A, $|A\rangle + h\nu \rightarrow |A^*\rangle$, then the ET from D^* to A is known as radiative energy transfer. This is also an important category of ET processes; however, they are usually not operative when the acceptor (or activator) is a lanthanide ion. This is because the oscillator strengths associated with 4f-4f transitions are very small ($\sim 10^{-6}$)[17-19], except for some transitions in Nd(Ⅲ) and Yb(Ⅲ), which preclude radiative absorption. Thus, for those interested in lanthanide ions, the dominant ET processes are nonradiative (or radiationless). Recently, the intramolecular ET processes in lanthanide complexes, namely, ligand-*Ln*(Ⅲ) transfer rates, were revised and reviewed[20]. Thus, the present review will focus on radiationless or nonradiative ET processes between lanthanide ions, *Ln*-*Ln*.

The main goal is to present a review for nonspecialists, providing sufficient concepts to critically ascertain the approximations involved in the equations of the energy transfer rate mechanisms. Enough details will be provided for a qualitative assessment of the main factors affecting the ET processes in *Ln*-*Ln* systems as well as to perform estimations and calculations of these ET rates. The original equations were reorganized to ease their applications as well as their interpretations. In the Supporting Information, a derivation of Fermi's golden rule is provided together with the physical constants and unit conversions, details matrix elements calculations, and dimensional analysis of the main quantities.

In the following sections, some concepts and equations involved in the quantum treatment of transitions will be present culminating in Fermi's golden rule for transition rates. This expression will then be particularized for nonradiative transitions between two lanthanide ions, namely, the *Ln*-*Ln* energy transfer rates. Detailed applications of these equations will be presented as tutorial examples for ET processes involved in the Yb(Ⅲ)-Er(Ⅲ) and Tb(Ⅲ)-Eu(Ⅲ) pairs.

2　Quantum Transitions

An energy transfer process can be regarded as a transition from a state representing the energy localized initially at the donor subsystem to another state characterized by the energy localized in the acceptor unit. This process can be described quantitatively by an energy transfer rate, that is, the probability of transition induced by a perturbation per unit of time, in units of s^{-1}, because the probability is dimensionless. Thus, to comprehend the equations for the ET rates, representations of the initial and final states are required, which will be addressed in detail later, as well as the transition probability between these states per unit of time.

For most transitions occurring at the molecular level, their rates can be quantitatively described by Fermi's golden rule. A detailed derivation of the expression for the transition rate, in particular Fermi's golden rule, can be found in many textbooks[21-22] and is provided in the Supporting Information. Here we will present the main equations and the approximations and assumptions employed.

Transitions at the molecular level are described by quantum mechanics. A system is described by its state represented by a (vector) state or wavefunction, which depends on the spatial and spin coordinates of its particles and on the time t. This state can be expressed as a linear combination of a complete set of eigenfunctions $\{\Psi_n(t)\}$ with corresponding energy eigenvalues $\{E_n\}$.

If the system is described by a time-independent Hamiltonian, *e. g.*, a molecule with contributions from the kinetic energy of the nuclei and electrons and Coulomb interactions between the charged particles (nuclei-nuclei, nuclei-electrons, and electrons-electrons), the time-dependent Schrödinger equation can be separated and have solutions $\Psi_n(t) = \psi_n e^{-iE_n t/\hbar}$, where ψ_n are the stationary (time-independent) eigenfunctions of this Hamiltonian. So, if the system is (prepared) at an eigenstate Ψ_m, with energy E_m, then it is stationary, $\Psi_m^*(t)\Psi_m(t) = \psi_m^* e^{iE_m t/\hbar}\psi_m e^{-iE_m t/\hbar} = \psi_m^*\psi_m = |\psi_m|^2$ = constant, and it

will remain in this state indefinitely. Thus, a perturbation $\hat{V}(t)$ is needed to promote a transition from this state to another state. This perturbation causes the temporal evolution of a non-stationary state $\Psi(t)$, which can still be represented as a linear combination of eigenfunctions $\{\Psi_n(t)\}$ with coefficients $\{c_n(t)\}$. As a result, the probability of finding the system at time t in state k is $\left|c_k(t)\right|^2 = c_k^*(t)c_k(t)$.

As a result of this perturbation, the system can be described by a Hamiltonian, $\hat{H}$, consisting of the time-independent Hamiltonian, $\hat{H}_0$, and the perturbation $\hat{V}(t)$, *i. e.*, $\hat{H} = \hat{H}_0 + \hat{V}(t)$. A procedure developed by Dirac starts by replacing the wavefunction $\Psi(t)$, in the time-dependent Schrödinger equation employing $\hat{H}$, by an expansion in terms of $\{\Psi_n(t)\}$ and $\{c_n(t)\}$. After applying the time derivative and the full Hamiltonian $\hat{H}$ on this expansion and projecting the resulting equation onto state k ('multiplication' or scalar product with the bra $\langle k|$), an exact equation for the time evolution $\dot{c}_n(t)$ is obtained. By integrating the resulting equation from $t = 0$, when the coefficients are $c_n(0)$, to the time t of interest, an exact expression for the coefficients $c_n(t)$ is derived, so the probability could, in principle, be calculated. Thus, a uniquely define exact solution is obtained when the boundary conditions, namely, the initial coefficients $c_n(0)$ are known. These conditions are usually expressed as $c_n(t = 0) = \delta_{ni}$, where i is the initial state, or $c_i(t = 0) = 1$ and $c_{n \neq i}(t = 0) = 0$.

However, the exact determination of the coefficient $c_k(t)$ requires all the coefficients, including $c_k(t)$, *i. e.*, the exact solution is a set of coupled integral equations. So, approximations and assumptions are needed to obtain a computable expression.

Suppose that the perturbation is so weak and applied during a time interval so short that all the coefficients remain close to their initial values and are approximated as $c_n(t) \cong 0$ for $n \neq i$ and $c_i(t) \cong 1$. This is the so-called first-order perturbation or first-order approximation and yields the following expression for the coefficients ($k \neq i$) at time t[21-22]:

$$c_k(t) \cong c_k^{(1)} = \frac{1}{\mathrm{i}\hbar}\int_0^t V_{ki}(t')e^{\mathrm{i}\omega_{ki}t'}\mathrm{d}t', \qquad (1)$$

where $\omega_{ki} = (E_k - E_i)/\hbar$ and the generic matrix element, V_{kn}, of the perturbation operator $\hat{V}$ is expressed as

$$V_{kn}(t) = \int\psi_k^*\hat{V}(t)\psi_n\mathrm{d}\tau \equiv \langle k|\hat{V}(t)|n\rangle, \qquad (2)$$

with the respect to the stationary eigenfunctions ψ_k and ψ_n. Notice that the first equality employs the integral representation of the matrix element, which is equivalent to that in the 'bra-ket' (or Dirac) notation.

3 Fermi's Golden Rule for Radiationless (or Nonradiative) Transitions

Several processes are induced by a coupling between subsystems or between states and radiation is not required, representing the so-called radiationless or nonradiative transitions. For example, in a time $t = 0$ the system (instantaneously) absorbs energy (*e. g.*, light absorption, mechanical or thermal excitations) and is promoted to an excited state, thus initiating a coupling or interaction. This is the initial condition of the system, and this excited state is its initial state i. The nonadiabatic electronic coupling or the spin-orbit coupling between the initial state i and another state k causes a radiationless transition from i to k, $i \rightarrow k$. Another example is a system of two uncoupled subunits, *e. g.*, donor and acceptor *D*-*A*. Upon excitation, at t=0, localized on the donor subsystem, the system can be represented as D^*-*A* and a coupling or interaction between *D* and *A* appears and promotes a nonradiative transition to another state that can lead to energy transfer or electron transfer, depending on the nature of the donor and acceptor, and on the initial and final states. In these radiationless transitions, the coupling or interaction initiated at t=0 does not depend explicitly on time, so it is constant in time: $\hat{V}(t) \equiv \hat{V}$ = constant.

Thus, for nonradiative energy transfer processes, a constant perturbation $\hat{V}$ (time-independent) is considered, which is turned on at $t = 0$ and off at $t = \tau$. For this perturbation, the coefficient describing state k at time $t \geqslant \tau$ becomes[21]:

$$c_k = -\frac{\mathrm{i}}{\hbar}V_{ki}\int_0^\tau e^{\mathrm{i}\omega_{ki}t}\mathrm{d}t,$$

$$V_{ki} = \int\psi_k^*\hat{V}\psi_i\mathrm{d}\tau \equiv \langle k|\hat{V}|i\rangle, \qquad (3)$$

where it was considered that the matrix element V_{ki} has a weak dependence on the quasi-continuum states around k. The duration of the perturbation, denoted as τ, should not be confused with the lifetime of an excited state, which is usually also denoted as τ.

The integral can be performed analytically, so the transition probability to state k is

$$P_k^i = \left|V_{ki}\right|^2 F_k^i\left(\omega_{ki}, \tau\right),$$
$$F_k^i\left(\omega_{ki}, \tau\right) = \frac{1}{\hbar^2}\frac{\sin^2\left(\omega_{ki}\tau/2\right)}{\left(\omega_{ki}/2\right)^2}. \quad (4)$$

This expression yields the same probability for the reverse transition: $P_k^i = P_i^k$, because $\left|V_{ki}\right|^2 = \left|V_{ik}\right|^2$ and $F_k^i = F_i^k$.

For $\tau \gtrsim 2\pi\hbar/E_k$, the function $F_k^i(\omega_{ki}, \tau)$ becomes sharply peaked, with the height of the peak around E_k increasing as $\tau^2/\hbar^2$ and width decreasing as $2\pi\hbar/\tau$, so the area of this peak is approximately $2\pi\tau/\hbar$, which grows linearly with τ. This indicates that a time τ after the initial coupling (or interaction) between the states or the subsystems, their energy eigenvalues will present dispersions of $\delta E = 2\pi\hbar/\tau$, which is consistent with the energy-time uncertainty principle because $\delta E\tau = 2\pi\hbar > \hbar/2$[21]. So, the final states after the perturbation are better described as nearly a continuum of energy values with a narrow distribution represented by a density of states, $\rho(E)$, which is the number of states per energy unit around energy E and $\rho(E)\mathrm{d}E$ is the number of (continuum) states in the range E to $E + \mathrm{d}E$[21-22]. In other words, the perturbation, represented by the interaction (or coupling), has generated many final states closely spaced in energy. For a molecular system, other mechanisms of energy dispersion will also be present, such as a distribution of closely spaced rotational-vibrational energy levels. Thus, if the final states have a density of states $\rho(E)$, then the total probability of transition to state k becomes an integral of $P_k^i\rho(E)\mathrm{d}E$ over all final states accessible under the influence of the perturbation:

$$P_{\bar{k}}^i = \int\left|V_{ki}\right|^2 F_k^i(\omega_{ki}, \tau)\rho(E_k)\mathrm{d}E_k \cong \left|V_{ki}\right|^2\rho(E_k)\int F_k^i(\omega_{ki}, \tau)\mathrm{d}E_k, \quad (5)$$

where the last approximation considers that the matrix element V_{ki} and the density of state $\rho(E_k)$ are constant in the integration range. Because the function $F_k^i(\omega_{ki}, \tau)$ is sharply peaked, the integrand has significant values only around E_k, which justifies the last approximation. This property of the function $F_k^i(\omega_{ki}, \tau)$ also allows for extending the integration from $-\infty$ to $+\infty$, so the last integral is just $2\pi\tau/\hbar$ and $P_{\bar{k}}^i$ has a linear dependence on τ, where $\bar{k}$ represents the summation over over the quasi-continuum (*e. g.*, rovibrational) contributions. . As a result, the transition rate $W_{i\to k} \equiv W_{ki}$ from an initial state i to a final state k, which is the change of the probability per unit of time, can be written as[21-22]:

$$W_{i\to k} \equiv W_{ki} = \frac{\mathrm{d}P_k^i}{\mathrm{d}t} \cong \frac{P_{\bar{k}}^i}{\tau} = \frac{2\pi}{\hbar}\left|V_{ki}\right|^2\rho\left(E_k\right). \quad (6)$$

This is called Fermi's golden rule and provides the rate of transition.

Despite this derivation being performed for constant perturbation, the same expression is obtained for periodic potentials that describe, for instance, the electromagnetic radiation.

For a proper application of this expression for the transition rate, it is important to present the approximations and assumptions as well as their consequences (see Supporting Information).

The task of applying Eq. (6) to a given process becomes (ⅰ) the proper representation of the initial and final states of the system, (ⅱ) defining and establishing the perturbation, and (ⅲ) determining the density of states.

The sharply peaked function $F_k^i(\omega_{ki}, \tau)$ appearing in Eq. (5) becomes a Dirac delta function at the $\tau \to \infty$ limit. As a result, the density of states $\rho(E_k)$ in Eq. (6) can be replaced by the delta function $\delta(E_k - E_i)$ for long τ[21-22]:

$$w_{ki} \cong \frac{2\pi}{\hbar}\left|V_{ki}\right|^2\delta\left(E_k - E_i\right),$$
$$W_{ki} = \int w_{ki}\rho\left(E_k\right)\mathrm{d}E_k. \quad (7)$$

This expression is known as state-to-state Fermi's golden rule. The delta function $\delta(E_k - E_i)$ expresses the condition that at the $\tau \to \infty$ limit, only transitions

that satisfy energy conservation can be caused by a secular (time-independent) interaction. The presence of $\delta(E_k - E_i)$ in Eq. (7) does not violate the energy-time uncertainty principle, because as $\tau \to \infty$, the energy dispersion $\delta E = 2\pi\hbar/\tau$ vanishes.

4 Rates of Energy Transfer Processes

As mentioned, the application of Eq. (6) for an energy transfer process between a donor and acceptor D-A requires the proper representation of the initial and final states. Usually, the subsystems D and A are considered uncoupled or weakly coupled, so that the state of the system can be represented by a (tensor) product of wavefunctions describing the subunits, namely, $\Psi \equiv \Psi_{DA} \cong \Psi_D \Psi_A$ or $|\Psi\rangle \equiv |DA\rangle \cong |D\rangle|A\rangle$. In this representation, the wavefunction Ψ_A depends on the spatial and spin coordinates of the nuclei and electrons constituting the acceptor and similarly Ψ_D the donor. Despite this simple notation, Ψ_D and Ψ_A represent multielectronic states that may require more than one determinant (multideterminantal) for an adequate description. Employing a single particle or monoelectronic representation may lead to improper descriptions and an unreliable picture of the energy transfer process.

The initial state $|i\rangle$ of an energy transfer process can be described by the donor at a higher or excited energy level and the acceptor at a lower or ground level denoted as $|i\rangle = |D^* A\rangle$. This represents the additional energy to be localized at the donor subsystem. Whereas the final state $|f\rangle$ would have this additional energy localized at the acceptor subunit and is represented as $|f\rangle = |DA^*\rangle$. As a result, the energy transfer process $|i\rangle \to |f\rangle$ can be pictured as a simultaneous deexcitation of the donor and excitation of the acceptor $|D^* A\rangle \to |DA^*\rangle$, without the presence of any photon or charge transferred. The ET process can then be represented as $|D^*\rangle|A\rangle \to |D\rangle|A^*\rangle$ to emphasize the independence of the subsystems. In addition, this representation allows for selection rules of the ET process. In other words, depending on the perturbation $\hat{V}$, a given deexcitation $|D^*\rangle \to |D\rangle$ or excitation $|A\rangle \to |A^*\rangle$ may not be allowed, so this energy transfer pathway is forbidden. However, it is important to remember that the selection rules will also depend on the nature of the donor and acceptor subsystems.

Because the D-A subunits are considered independent, the perturbation can be promptly and easily pictured as the interaction between these subsystems. So, the perturbation $\hat{V}$ can be represented by the Coulomb (or electrostatic) interactions between electron densities and nuclear charges of the donor and the acceptor. This perturbation leads to a mechanism known as multipolar[23] or, more restricted, dipolar or Förster[24]. On the other hand, approximating the wavefunction of the system by a (tensor) product causes the electrons of the donor to be distinguishable from the electrons of the acceptor, which violates the indistinguishability and antisymmetry principles of quantum mechanics. So, the exchanges between the electrons of the donor and the acceptor can be regarded as a perturbation of the D-A subunits. This perturbation can be described by an exchange operator and originates a mechanism known as exchange or Dexter[25].

A step further in the development of a workable expression for the energy transfer rate can be taken by realizing that, usually, the time scale of the nuclear motion is much longer than of the electronic motion. As a result, the molecular wavefunction can be approximately factored into a product of electronic and nuclear wavefunctions. This is the well-known Born-Oppenheimer approximation, which has been used since the dawn of quantum mechanics and its successes and limitations are well-established[26-27]. So, the wavefunctions describing the initial state with the energy localized at the donor, $|i\rangle = |D^* A\rangle$, and the final state related to the energy localized at the acceptor, $|f\rangle = |DA^*\rangle$, can be approximated as

$$|i\rangle \cong |D^* A\rangle_e |D^* A\rangle_{nuc},$$
$$|f\rangle \cong |DA^*\rangle_e |DA^*\rangle_{nuc}, \quad (8)$$

where $|D^* A\rangle_e \equiv \psi_e(D^* A)$ is the electronic wavefunction

of the donor in an excited state and the acceptor in the ground state, while $\left|DA^*\right\rangle_e \equiv \psi_e(DA^*)$ is the electronic wavefunction of the donor in the electronic ground state and the acceptor in an excited state. These electronic states have corresponding nuclear wavefunctions represented as $\left|D^*A\right\rangle_{nuc} \equiv \psi_{nuc}(D^*A)$ and $\left|DA^*\right\rangle_{nuc} \equiv \psi_{nuc}(DA^*)$, which are usually described as vibrational wavefunctions. It is important to emphasize that the electronic wavefunction $\left|X\right\rangle_e \equiv \psi_e(X)$ is a parametric function of the nuclear positions $\boldsymbol{R}_\alpha$, with α being the label of each nucleus in the D-A system. As a result, any expectation value concerning the electronic wavefunction will be a function of the set $\{\boldsymbol{R}_\alpha\}$, namely, $A(\{\boldsymbol{R}_\alpha\}) = \langle\hat{A}\rangle = \int\psi_e^*(X)\hat{A}\psi_e(X)\mathrm{d}\tau \equiv \langle X|\hat{A}|X\rangle_e$. Substitution of these factored representations of the initial and final states in Eq. (6) yields the following expression for the energy transfer rate

$$W_{ET} \cong \frac{2\pi}{\hbar}\left|V_{fi}\right|^2 F,$$

$$V_{fi} = \int\psi_e^*(DA^*)\hat{V}\psi_e(D^*A)\mathrm{d}\tau \equiv \left\langle DA^*|\hat{V}|D^*A\right\rangle_e, \quad (9)$$

where V_{fi} is the electronic matrix element due to the time-independent part $\hat{V}$ of the perturbation operator, while the F-factor includes contributions from the overlap of the nuclear wavefunctions, $\int\psi_{nuc}^*(DA^*)\cdot\psi_{nuc}D^*A)\mathrm{d}\tau \equiv (\langle D^*A|DA^*\rangle$, and from the density of states $\rho(E)$. This separation into an electronic contribution V_{fi} and a F-factor is possible only if the time-independent perturbation $\hat{V}$ acts in the electronic (spatial and spin) coordinates, so V_{fi} is a function of the nuclear positions $\boldsymbol{R}_\alpha$, $V_{fi} \equiv V_{fi}(\{\boldsymbol{R}_\alpha\})$. Notice that in the wavefunction representation of the matrix element, the notation ψ_e^* represents the complex conjugate of the function ψ_e, whereas DA^* or D^*A represents the acceptor or the donor in an excited electronic state. This confusion does not arise in the 'bra-ket' notation.

So far, the proposed model, expressed in Eq. (9), to describe energy transfer processes is general and can be applied to intermolecular D…A organic and/or inorganic pairs[28-29] as well as energy transfer in intramolecular D-A pair such as lanthanide complexes L-*Ln*(ligand-lanthanide ion)[20,30-33] and lanthanide-lanthanide ion pairs Ln_D-Ln_A[34-37]. For the latter case, it is important to distinguish two situations: Ln_D-L-Ln_A, when there are bridging ligands between the lanthanide ions; and Ln_D-Ln_A, when no ligands bridge the ions. The case of Ln_D-L-Ln_A will not be considered here because the direct energy transfer pathways between the lanthanide ions are very inefficient compared to the ligand-lanthanide energy transfer pathways. So, most likely this case involves nonradiative energy transfer processes between the ligands and the lanthanide ions. Recently, the theoretical modeling of intramolecular ligand-lanthanide energy transfer was reviewed[20]. So, here the focus will be on the direct energy transfer in Ln_D-Ln_A pairs with no bridging ligands will be described.

5 Energy Transfer Rates Between Lanthanide Ions

A quantitative description of the nonradiative energy transfer between lanthanide ions (*Ln*-*Ln* ET) was developed in the early 1970s[38], after the success of the Judd-Ofelt theory for the 4f-4f transition intensities[39-40] and way before the development of the ligand-lanthanide ET model[20,32,41]. This sequence of events may be explained by the very similar nature of the donor and acceptor states in the *Ln*-*Ln* ET, in contrast to the very dissimilar nature of the states involved in ligand-lanthanide ET. Lanthanide ions have a unique feature related to the shielding of the N electrons in the 4f subshell, $4f^N$. Because the filled subshells $5s^25p^6$ are more radially external than the $4f^N$ subshell, the electronic density of $5s^25p^6$ shields the 4f electrons from the interactions with the surroundings (*e. g.*, ligating atoms, ligands, ions, lattice, solvent, *etc.*) of the lanthanide. As a result, the 4f states are practically those of the free-ion, where the effects of the surroundings can be treated as a small perturbation, if necessary. This feature was explored in the development of the Judd-Ofelt theory, and the successes of this formulation validate this picture of the 4f states. Therefore, donor

and acceptor states in the energy transfer processes between 4f levels of lanthanide ions are well-defined and several theoretical tools developed previously could be employed. These *Ln*-*Ln* ET processes can be pictured as an excited state within the $4f^{N_D}$ configuration of the donor lanthanide being deexcited to a lower level (usually the ground state) and its energy is transferred to the acceptor lanthanide causing an excitation within its $4f^{N}$ configuration. Because the 4f donor and acceptor states are well localized on each lanthanide, the donor-acceptor distance is taken as the distance between the lanthanide ions. This feature is not present in a ligand-*Ln* system, because the states of the ligand are usually delocalized, the donor-acceptor distance is much more difficult to define and determine.

Because of the localized nature of the 4f states, the donor and acceptor electronic wavefunctions can be approximately treated as independent or uncoupled, that is,

$$\begin{aligned} \left|D^{*}A\right\rangle_{e} &\equiv \psi_{e}^{*}\left(DA^{*}\right) \cong \left|D^{*}\right\rangle\left|A\right\rangle, \\ \left|\mathrm{DA}^{*}\right\rangle_{e} &\equiv \psi_{e}^{*}(\mathrm{DA}^{*}) \cong \left|\mathrm{D}\right\rangle\left|\mathrm{A}^{*}\right\rangle, \end{aligned} \tag{10}$$

where $\left|D^{*}\right\rangle$ and $\left|D\right\rangle$ represent the electronic wavefunction of the isolated donor in the excited and ground states, respectively, whereas $\left|A\right\rangle$ and $\left|A^{*}\right\rangle$ of the isolated acceptor in the ground and excited states. As a result, the perturbation operator $\hat{V}$ in Eq. (9) becomes well defined, namely, it represents the interactions between these two independent D-A subunits. The immediate interaction is the electron repulsions between the electronic densities of $\left|D^{*}\right\rangle\left|A\right\rangle$ and $\left|D\right\rangle\left|A^{*}\right\rangle$. This has a classical analogue related to Coulomb interactions between the charge densities and can be represented by the following operator

$$\hat{V}_{\mathrm{C}} = \sum_{i\in \mathrm{D}}\sum_{j\in \mathrm{A}}\frac{e^{2}}{\left|\boldsymbol{r}_{i}-\boldsymbol{r}_{j}\right|} \equiv \sum_{i\in \mathrm{D}}\sum_{j\in \mathrm{A}}\frac{e^{2}}{r_{ij}}, \tag{11}$$

where $\boldsymbol{r}_i$ and $\boldsymbol{r}_j$ are the position vectors of electrons i (belonging to the donor) and j (belonging to the acceptor), respectively.

Another more subtle interaction comes from the principles of quantum mechanics, which has no classical analogue. In the approximation expressed by Eq. (10), it is implicitly assumed that the donor has a fixed number of electrons, *e. g.*, N_{D}, as well as the acceptor has N_{A}-electrons. However, when these subsystems interact with each other, the electrons of the donor must become indistinguishable from the electrons of the acceptor, as a principle of quantum mechanics. This can be accomplished by an exchange operator that permutes the indices (or labels) of each electron of the donor with each electron of the acceptor, which can be represented by the following operator

$$\hat{V}_{\mathrm{ex}} = \sum_{i\in \mathrm{D}}\sum_{j\in \mathrm{A}}\frac{e^{2}}{r_{ij}}P_{ij},\ P_{ij} = \frac{1}{2} + \hat{\boldsymbol{s}}_{i}\cdot\hat{\boldsymbol{s}}_{j}, \tag{12}$$

where $\hat{\boldsymbol{s}}_i$ and $\hat{\boldsymbol{s}}_j$ are the spin operators of electrons i and j. It is important to realize that the wavefunctions of the isolated donor and acceptor are normalized and antisymmetrized, so they individually satisfy the principles of quantum mechanics.

The electronic wavefunctions of 4f states of an isolated lanthanide ion are accurately described by the total electronic angular momentum quantum number J and additional quantum numbers ψ. Thus, the initial $\left|D^{*}\right\rangle\left|A\right\rangle$ and final $\left|D\right\rangle\left|A^{*}\right\rangle$ states, Eq. (10), in the ET process are represented as $\left|\psi_{\mathrm{D}}^{*}J_{\mathrm{D}}^{*}\right\rangle\left|\psi_{\mathrm{A}}J_{\mathrm{A}}\right\rangle$ and $\left|\psi_{\mathrm{D}}J_{\mathrm{D}}\right\rangle\left|\psi_{\mathrm{A}}^{*}J_{\mathrm{A}}^{*}\right\rangle$. Notice that the projection M_J of the angular momentum J is also an appropriate quantum number. In addition, it is possible to represent these wavefunctions as a linear combination of the wavefunctions represented in the total spin S and orbital L angular momenta (and their projections, M_S and M_L) basis as the so-called intermediate coupling scheme. This transformation is quite convenient because it allows the choice of a diagonal matrix representation of the operator of interest.

Once the wavefunctions describing the initial and final states have been properly represented, the matrix element involving the perturbation operator $\hat{V} = \hat{V}_{\mathrm{C}} + \hat{V}_{\mathrm{ex}}$ can be determined. Notice that this operator involves the two-electron interaction e^{2}/r_{12}, which can be expanded in terms of the spherical harmonics or equivalently in terms of Racah's irreducible

spherical tensor operators[23,42]. This allows the factorization of the matrix element into radial and angular parts, where this latter part can be calculated analytically. As a result, the following equations for the energy transfer rates between lanthanide ions can be obtained[16,34-37,43] and classified the dipole-dipole, $W_{\text{d-d}}$

$$W_{\text{d-d}} = \frac{4\pi}{3\hbar}\frac{S_{\text{d}}^{\text{D}} S_{\text{d}}^{\text{A}}}{R_{\text{DA}}^{6}} F, \tag{13}$$

the dipole-quadrupole and quadrupole-dipole, $W_{\text{dq-qd}}$,

$$W_{\text{dq-qd}} = \frac{\pi}{\hbar}\frac{(S_{\text{d}}^{\text{D}} S_{\text{q}}^{\text{A}} + S_{\text{q}}^{\text{D}} S_{\text{d}}^{\text{A}})}{R_{\text{DA}}^{8}} F, \tag{14}$$

the quadrupole-quadrupole, $W_{\text{q-q}}$,

$$W_{\text{q-q}} = \frac{28\pi}{5\hbar}\frac{S_{\text{q}}^{\text{D}} S_{\text{q}}^{\text{A}}}{R_{\text{DA}}^{10}} F, \tag{15}$$

the magnetic dipole-magnetic dipole $W_{\text{md-md}}$,

$$W_{\text{md-md}} = \frac{4\pi}{3\hbar}\frac{S_{\text{md}}^{\text{D}} S_{\text{md}}^{\text{A}}}{R_{\text{DA}}^{6}} F, \tag{16}$$

and the exchange, W_{ex}, mechanisms

$$W_{\text{ex}} = \frac{2\pi}{\hbar}\left[\left(\frac{e^2}{R_{\text{DA}}}\right)\rho_{\text{ff}}^{2}\right]^2 F, \tag{17}$$

where S_{d} (in erg·cm^3) is the modified forced electric dipole strength

$$S_{\text{d}}^{x} = \frac{e^2\left(1-\sigma_1^{x}\right)^2}{2J_x+1}\sum_{K=2,4,6}\Omega_K^{x}\left\langle \psi_x^{*}J_x^{*}\middle\| U^{(K)}\middle\|\psi_x J_x\right\rangle^2, \tag{18}$$

while S_{q} (in erg·cm^5) is the modified quadrupole strength

$$S_{\text{q}}^{x} = \frac{e^2(1-\sigma_2^{x})^2}{2J_x+1}\left\langle f\middle\| C^{(2)}\middle\| f\right\rangle^2 \times \left\langle r^2\right\rangle_x^2\left\langle \psi_x^{*}J_x^{*}\middle\| U^{(2)}\middle\|\psi_x J_x\right\rangle^2, \tag{19}$$

whereas S_{md} (in erg·cm^3) is the magnetic dipole strength analogue

$$S_{\text{md}}^{x} = \frac{\mu_{\text{B}}^2(1-\sigma_{\text{md}}^{x})^2}{(2J_x+1)}\left\langle \psi_x^{*}J_x^{*}\middle\|\hat{M}\middle\|\psi_x J_x\right\rangle^2, \quad \hat{M}\equiv\hat{L}+g_S\hat{S}, \tag{20}$$

with x = A for the acceptor and x = D for the donor, $J_x = J_{\text{D}}^{*}$ being the total angular momentum quantum number of the excited state of the donor or $J_x = J_{\text{A}}$ of the ground state of the acceptor, and g_S = 2.002 319 3 being the electron spin g-factor[44]. See the Supporting Information for dimensional analysis and unit conversion.

The total energy transfer rate will be a summation of each contribution in Eqs. (13)-(17). Usually, there is one contribution that dominates this sum, however, there are exceptions, and the relative contributions change strongly with the donor-acceptor distance, R_{DA}.

It is important to emphasize that S_{d} is denoted as *forced electric* dipole strength analogue because *only the forced electric dipole* (FED) mechanism contributes to the calculation of Ω_K. This is due to the contribution of the opposite parity configuration mixing by the odd components of the ligand field to the intensity parameters Ω_K, like in the Judd-Ofelt theory[38].

These equations are the same as those published in the revisited versions of the energy transfer rates between lanthanide ions[34,36-37]. However, those involving multipole and magnetic dipole mechanisms were rearranged and separated into more symmetrical and easily interpretable forms. In addition, these separations allow a stepwise calculation of the contributing terms, which can assist the analysis of the transfer rates and determine if there are dominant contributions from either donor or acceptor.

The energy transfer rates are expressed in terms of well-defined and calculable quantities. It must be emphasized that the choice of the two-electron interaction as e^2/r_{12}, implies that the CGS system of units is employed. The quantities in these expressions depend on physical constants and other properties independent of the nature of the lanthanide ion:

· $\hbar = h/(2\pi)$ is the reduced Planck constant (see the Supporting Information for the values of the physical constants and unit conversion),

· e is the elementary charge in esu,

· $\mu_{\text{B}} = e\hbar/(2m_e c)$ is the Bohr magneton,

· $\left\langle f\middle\| C^{(2)}\middle\| f\right\rangle = -1.366$ is the one-electron doubly reduced spherical tensor matrix element (dimensionless)[23],

on intrinsic quantities of the lanthanide ion:

· J_{D}^{*} is the total angular momentum quantum number of the excited state of the donor and J_{A} of the ground state of the acceptor,

· $\left\langle \psi^* J^* \middle\| U^{(K)} \middle\| \psi J \right\rangle$ (dimensionless) are the doubly reduced matrix elements of the unit irreducible tensor operator $U^{(K)}$ of rank K evaluated in the intermediate coupling scheme. Their square, $\left\langle \psi^* J^* \middle\| U^{(K)} \middle\| \psi J \right\rangle^2$, are often abbreviated as $U^{(K)}$[45] or $U(K)$[46] and tabulated values can be found in reference [47], *e. g.*, Eu(Ⅲ) has $\left\langle {}^7\mathrm{F}_2 \middle\| U^{(2)} \middle\| {}^5\mathrm{D}_0 \right\rangle^2 = 0.0032$ and $\left\langle {}^7\mathrm{F}_4 \middle\| U^{(4)} \middle\| {}^5\mathrm{D}_0 \right\rangle^2 = 0.0023$,

· $\left\langle \psi^* J^* \middle\| \hat{M} \middle\| \psi J \right\rangle$ (dimensionless), $\hat{M} \equiv \hat{L} + g_S \hat{S} \cong \hat{L} + 2\hat{S}$ is the doubly reduced matrix element of the angular $\hat{L}$ and spin $\hat{S}$ operators calculated in the intermediate coupling scheme[48-50], have typical values of 0.1–0.6 for states with different L and S terms[37] and assume high values into the same L and S terms (*e. g.*, Tb(Ⅲ) has $\left| \left\langle {}^7\mathrm{F}_5 \middle\| \hat{M} \middle\| {}^7\mathrm{F}_6 \right\rangle \right| = 4.38$)[51]. It is important to emphasize that this matrix element is also expressed in units of $\hbar$, in which case, the Bohr magneton μ_B cannot include $\hbar$,

· $\langle r^t \rangle \equiv \langle 4\mathrm{f}|r^t|4\mathrm{f} \rangle$ is the expectation value (integral) of r^t with respect to the 4f radial function and the values for t =2, 4, and 6 can be found in Ref. [52], *e. g.*, $\langle r^2 \rangle$ are 0.997, 0.893, 0.710, 0.773 a. u. for Eu(Ⅲ), Tb(Ⅲ), Yb(Ⅲ), and Er(Ⅲ), respectively[52],

· $\Omega_K \equiv \Omega_K(\mathrm{FED})$ is the forced electric dipole contribution to the intensity parameter of rank K, in units of 10^{-20} cm^2[20,34,36],

on the surroundings of the lanthanide ion:

· $(1 - \sigma_k)$, with k = 1 and 2, is the shielding factor for donor and acceptor approximated as[34,53-54]

$$(1 - \sigma_k) = \rho(2\beta)^{k+1}, \tag{21}$$

where ρ is the overlap integral between the valence subshells of the ligating atom and the 4f subshell of the lanthanide ion and $\beta = 1/(1 \pm \rho)$[53,55],

· σ_{md} is the shielding factor, for donor and acceptor, which shields the magnetic dipole interactions,

on the lanthanide pair:

· R_{DA} is the distance between the lanthanides,

$$R_{\mathrm{DA}} = \sqrt{(x_\mathrm{D} - x_\mathrm{A})^2 + (y_\mathrm{D} - y_\mathrm{A})^2 + (z_\mathrm{D} - z_\mathrm{A})^2}, \tag{22}$$

with $(x_\mathrm{D}, y_\mathrm{D}, z_\mathrm{D})$ and $(x_\mathrm{A}, y_\mathrm{A}, z_\mathrm{A})$ being the Cartesian coordinates of the donor and acceptor centers, respectively,

· ρ_{ff} is the overlap integral between the 4f subshells of the donor and acceptor lanthanide ions[53].

The last quantity to determine the ET transfer rates is the F-factor in Eq. (9), which includes contributions from the nuclear wavefunctions and the density of states. It is important to recall that when the donor subunit is excited to generate the initial state in the energy transfer process, the energy eigenvalues will be broadened and will have a quasi-continuum behavior that is described by the density of states of the donor $\rho_\mathrm{D}(E)$ and of the acceptor $\rho_\mathrm{A}(E)$. In the original model for the nonradiative energy transfer between organic species *via* the dipole-dipole mechanism[24], this factor was assigned to and determined as the spectral overlap between the absorption band of the acceptor and the emission band of the donor. As a result, the emission spectrum of the donor and the absorption spectrum of the acceptor are recorded separately and properly rescaled to determine the area under which these spectra overlap. However, this requires the spectra of the isolated donor and acceptor, which might not be viable, as well as a delicate procedure for determining the area of the spectral overlap. This would also preclude the development of a quantitative and predictive model. Considering that the density of states $\rho_\mathrm{D}(E)$ and $\rho_\mathrm{A}(E)$ are Gaussian functions, then the area of their overlap can be expressed as a sum of two error functions that depend on the widths of the Gaussian functions, their energy maxima, and the point of their intersection. Despite this area being calculable, there is not an analytical expression for it, which requires numerical modeling.

It should be noticed that a typo occurred in the expression of $W_{\mathrm{md\text{-}md}}$ in previous publications[16,37,56], where σ_1^x was used instead of σ_{md}^x as shown in Eq. (20). Indeed, because the electric dipole interactions, which are shielded by electron densities represented as σ_1^x, have different nature than the magnetic dipole interactions, the shielding of these interactions,

represented as σ^{x}_{md}, should not be the same. Hence, the introduction of the new notation σ^{x}_{md}. However, because the shielding of the 4f electrons by the remaining electrons of the lanthanide ion and of the ligands involves closed-shells (*e. g.*, $5s^2 5p^6$), then it is expected that the magnetic shielding σ^{x}_{md} should be very small. This reasoning, associated with the difficulties in modeling σ^{x}_{md}, has prompted the complete neglect of σ^{x}_{md} in the equation for $W_{md\text{-}md}$ [57-58] or to consider $\sigma^{x}_{md} \approx 0$ in the calculations of $W_{md\text{-}md}$ [16,37,56], which will cause a slight overestimation of the $W_{md\text{-}md}$ rate.

During the study of the plasmon effects on the luminescence of lanthanide ions, an alternative model was developed to determine the contributions of the density of states $\rho_D(E)$ and $\rho_A(E)$ to the *F*-factor[59]. Later, the overlaps of the vibrational states were taken into consideration to develop a more complete formulation of the *F*-factor, which becomes a function of the temperature by assuming a Boltzmann distribution for the vibrational states of the initial and final electronic states[20,34]. This formulation is relevant because it explicitly accounts for the creation of phonons when the donor state has energy higher than the acceptor. It also accounts for the annihilation of phonons when the donor state is below in energy relative to the acceptor state because the energy mismatch must be compensated by phonons[20]. By considering the bands of the donor and acceptor, $\rho_D(E)$ and $\rho_A(E')$, have Gaussian profiles, an analytical expression for the integral of a product of two Gaussian functions can be obtained[60]. This comes from the fact that a product of two Gaussian functions is a well-defined Gaussian function, whose define integral has analytical expression and the *F*-factor can be expressed approximately as (in erg^{-1})[34]

$$F = \frac{Y}{\left(\gamma_D^2 + \gamma_A^2\right)^{1/2}} \times e^{-(\Delta/\gamma_D)^2 \Gamma} G(\Delta, T), \quad (23)$$

where

$$\Gamma = \left[1 - \frac{1}{1 + \left(\gamma_D/\gamma_A\right)^2}\right] \ln 2, \quad (24)$$

$$Y = \left(\frac{\ln 2}{\pi}\right)^{1/2} \frac{1}{ch},$$

with γ_D and γ_A being the bandwidths at half-height (in cm^{-1}) of the donor and acceptor, respectively, so $2\pi c\hbar\gamma_x$ has units of energy (in erg), Δ (in cm^{-1}) being the energy difference (mismatch) between the donor and acceptor states, $\Delta = E_D - E_A$, and $Y = 2.3646184 \times 10^{15}\ cm^{-1} \cdot erg^{-1}$. The function $G(\Delta,T)$ in Eq. (23) collects contributions from the overlaps of the vibrational wavefunctions, which can be expressed in terms of the Huang-Rhys parameters with dependence on the average vibrational quantum number and on the number of phonons required for energy conservation. An approximated expression for this function is

$$G(\Delta, T) = \begin{cases} 1, & \Delta > 0 \\ e^{\Delta/(k_B T)}, & \Delta < 0 \end{cases}, \quad (25)$$

which represents an approximation to the multiphonon mechanism used to compensate for the energy conservation, with k_B being the Boltzmann constant.

This reorganized form of the *F*-factor shows explicitly its dependence on the energy mismatch Δ and the bandwidths $\hbar\gamma_D$ and $\hbar\gamma_A$. For instance, in the case of *Ln-Ln* energy transfer, the bandwidths are narrow and practically the same, $\gamma_D \cong \gamma_A \equiv \gamma$, so $F = (Y/\gamma\sqrt{2})e^{-(\Delta/\gamma)^2(\ln 2)/2} G(\Delta)$. For narrow bands, the restriction on the energy mismatch Δ is quite severe. For instance, $\gamma \cong 200\ cm^{-1}$ gives $F \cong 8 \times 10^{12} e^{-0.35(\Delta/\gamma)^2}\ erg^{-1}$, for $\Delta > 0$. If $\Delta \cong 1\,000\ cm^{-1} = 5\gamma$, then $e^{-0.3466 \cdot 5^2} \sim 10^{-4}$ and $F \sim 10^9\ erg^{-1}$; however, if $\Delta \cong 2\,000\ cm^{-1} = 10\gamma$, then $e^{-0.3466 \cdot 10^2} \sim 10^{-15}$ and $F \sim 10^{-2}\ erg^{-1}$. So, a twofold increase in Δ leads to a 10^{11} decrease of *F*, because of the quadratic dependence on Δ in the argument of the exponential. This situation is quite distinct from that involving a sensitizer with a broad band, where $\gamma_D \gg \gamma_A$. In this case, the *F*-factor becomes $F = (Y/\gamma_D) e^{-(\Delta/\gamma_D)^2 \ln 2} G(\Delta)$. So, for a donor bandwidth of $\gamma_D \cong 2\,000\ cm^{-1}$ and $\Delta \cong 6\,000\ cm^{-1} = 3\gamma_D$, then $F \sim 2 \times 10^9\ erg^{-1}$. Despite this energy mismatch Δ being six times larger than that of narrow bands, the *F*-factor is the same order of magnitude because it corresponds to three times the broader

bandwidth, whereas in the latter case it corresponds to five times the narrower bandwidth.

The dependence of the F-factor on the energy mismatch, bandwidths, and temperature is depicted in the following Figs.

Fig. 1 shows that the F-factor is slightly asymmetric because the function $G(\Delta,T)$ differs when $\Delta < 0$ or $\Delta > 0$ (Eq. 25). For very narrow bandwidths values (*e. g.*, $\gamma_D = \gamma_A \approx 100\ cm^{-1}$), the F-factor assumes high values only if Δ is in the same order as bandwidths.

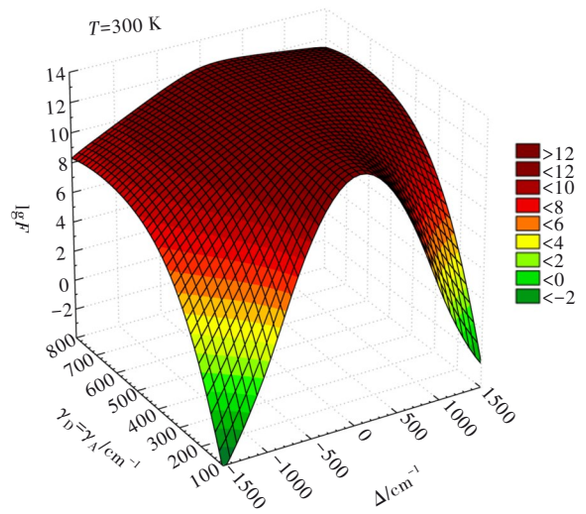

Fig.1 Dependence of the F-factor on the energy mismatch Δ and the bandwidth γ, for $\gamma_D = \gamma_A = \gamma$ and temperature T = 300 K. Graph in linear scale in Fig.S1.

Temperature effects on the energy transfer rates can be rationalized from the changes of the F-factor. Thus, two outcomes (direct and indirect) are expected: the energy mismatch barrier in the $G(\Delta,T)$ when $\Delta<0$ (direct) and the widening of the bandwidths due to the temperature rising (indirect). Fig. 2 shows the F-factor behaves as a function of temperature (direct) and of Δ, for fixed values of $\gamma_D = \gamma_A \approx 400\ cm^{-1}$. For the temperature effects on the bandwidth broadening, consider the following hypothetical case: a co-doped Nd(Ⅲ),Yb(Ⅲ)-containing material at an initial temperature T_i presents $\gamma_D(T_i) = \gamma_A(T_i) \approx 300\ cm^{-1}$ for a pair of donor and acceptor transitions (*e. g.*, Nd(Ⅲ) $^4G_{5/2} \rightarrow {}^4I_{15/2}$ as donor and Yb(Ⅲ) $^2F_{7/2} \rightarrow {}^2F_{5/2}$ as acceptor, with $\Delta \cong 1\ 100\ cm^{-1}$[47]), and the sample is uniformly heated to a final temperature T_f and both bandwidths increase by 50 cm^{-1}, so ($\gamma_D(T_f) = \gamma_A(T_f) \approx 350\ cm^{-1}$). According to Eq. (23) and approximating $\Delta \cong 1\ 000\ cm^{-1}$ (as illustrated in Fig. 3), the F-factor increases from 1.18×10^{11} to $2.82\times10^{11}\ erg^{-1}$.

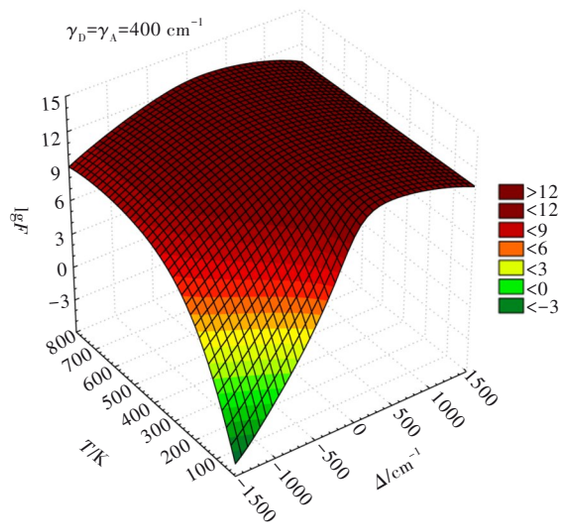

Fig.2 Dependence of the F-factor on the energy mismatch Δ and the temperature. $\gamma_D = \gamma_A = 400\ cm^{-1}$. Graph in linear scale in Fig.S2.

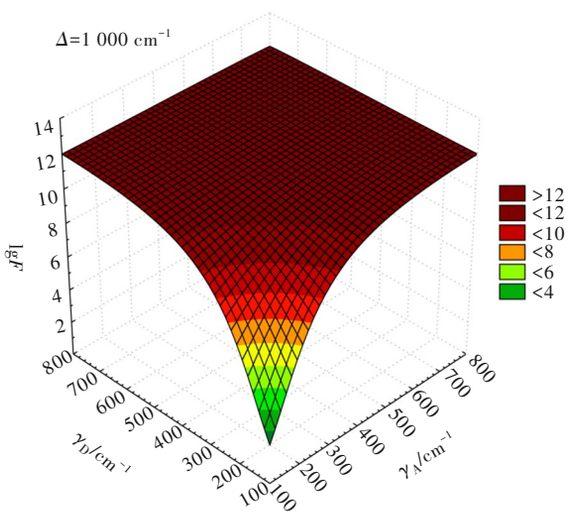

Fig.3 Dependence of the F-factor on the energy bandwidths of the donor (γ_D) and the acceptor (γ_A). Δ = 1 000 cm^{-1}. Graph in linear scale in Fig.S3.

Notice that the graph in Fig. 3 presents symmetry with respect to the interchange of γ_D and γ_A values, which is not evident in Eqs. (23) and (24) because of the $e^{-(\Delta/\gamma_D)^2\Gamma}$ term. However, it makes sense once the Dirac delta function acting in k and i states should be the same when the order of states is reversed, *i. e.*, $\delta(E_k - E_i) = \delta(E_i - E_k)$ in Eq. (7).

6 Selection Rules for Energy Transfer Rates

Lanthanide ions have a wealthy number of levels in the optical region that can be active in energy transfer processes. So, the number of ET pathways between two lanthanide ions can be substantially large and the selection rules are important to exclude those pathways that are null. In fact, the selection rules of the J quantum number, together with the energy mismatch Δ, in Eq. (23), are very useful to select the donor and acceptor states for adequate ET pathways.

The exchange contribution, Eq. (17), to the ET rate *does not have selection rules* for the J quantum number, that is, it always present, regardless of the donor or acceptor states. This is particular to lanthanide-lanthanide ET processes because in this case, the isotropic contribution does not vanish, so no dependence on the angular momentum appears. For the case of ligand-lanthanide ET processes, because the ligand states are usually restricted to singlets and triplets, with a singlet ground state, the contribution from the spin operator vanishes and only transitions with $|\Delta J| = 0$ or 1 are allowed (nonvanishing)[20]. Despite this lack of selection rules, the exchange contribution is strongly dependent on the lanthanide-lanthanide distance, R_{DA}, because of R_{DA}^{-2} in Eq. (17), and, mainly of ρ_{ff}^{4} dependence. Indeed, the overlap integral between 4f-4f radial functions, ρ_{ff}, decreases rapidly with the lanthanide-lanthanide distance (Fig. 4)[53]. As a result, depending on the value of the F-factor, the exchange contribution, W_{ex}, can be promptly ruled out and would be considered mostly when the other contributions are null.

In the case of the multipolar mechanisms, $W_{d\text{-}d}$, $W_{dq\text{-}qd}$, and $W_{q\text{-}q}$, the selection rules are: $|J^* - J| \leqslant K \leqslant J^* + J$. These come from the fact that these rates will vanish when the dipole S_d^x or quadruple S_q^x strengths are null. On the other hand, these quantities will be null when all reduced matrix elements $\langle \psi_x^* J_x^* \| U^{(K)} \| \psi_x J_x \rangle$ are zero, hence these selection rules. For instance, consider the $^5D_4 \rightarrow {}^7F_5$ transition of Tb

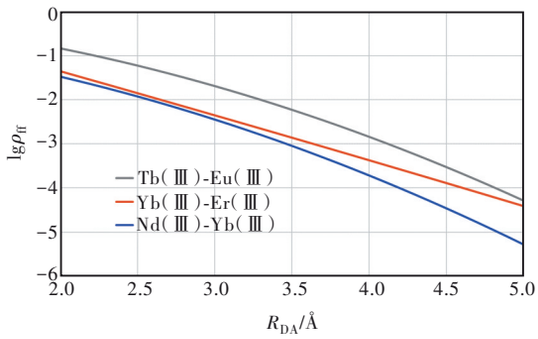

Fig.4　4f-4f overlap integrals (lg scale of ρ_{ff}) as a function of *Ln-Ln* distance (R_{DA} in Å) for the Tb(Ⅲ)-Eu(Ⅲ), Yb(Ⅲ)-Er(Ⅲ), and Nd(Ⅲ)-Yb(Ⅲ) pairs. DFT calculations with BP86 functional[61-62], TZ2P basis set[63], and the inclusion of ZORA scalar relativistic effects[64-65] were performed in the ADF program[66]. Parametric functions derived from these calculations for any *Ln-Ln* pair can be found in reference[53]. Graph in linear scale in Fig.S4.

(Ⅲ) as a donor state, then $|J_D^* - J_D| = 1$ and $J_D^* + J_D = 9$, so $1 \leqslant K \leqslant 9$ which covers all possible values of K and increases the chance of having nonzero matrix elements. On the other hand, if the acceptor state is the $^7F_0 \rightarrow {}^5D_1$ transition of Eu(Ⅲ), then $|J_A^* - J_A| = 1$ and $J_A^* + J_A = 1$, so $K = 1$ and the transition is forbidden because matrix elements $\langle \psi_x^* J_x^* \| U^{(1)} \| \psi_x J_x \rangle$ are zero. However, these selection rules may be slightly relaxed by the J-mixing effect, providing very small values of $\langle \psi_x^* J_x^* \| U^{(2)} \| \psi_x J_x \rangle^2 \approx 0.0032 \times 0.05^2$ for the specific cases involving the Eu(Ⅲ) $^7F_0$ level. Therefore, this effect is negligible in the energy transfer between lanthanide ions.

So, the contributions from multipolar mechanisms, $W_{d\text{-}d}$, $W_{dq\text{-}qd}$, and $W_{q\text{-}q}$, to the ET rate *via* the pathway Tb(Ⅲ) $^5D_4 \rightarrow {}^7F_5$ to Eu(Ⅲ) $^7F_0 \rightarrow {}^5D_1$ are null. However, this pathway is allowed by the exchange mechanism and might be allowed by the magnetic dipole mechanism. Hence, for the multipolar mechanisms, another acceptor state of Eu(Ⅲ) needs to be considered, *e. g.*, $^7F_1 \rightarrow {}^5D_1$. In this case, $|J_A^* - J_A| = 0$ and $J_A^* + J_A = 2$, so $K = 2$ and the $^7F_1 \rightarrow {}^5D_1$ transition is allowed because matrix element $U^{(2)}$ of Eu(Ⅲ) is nonzero.

The remaining mechanism for ET between lanthanide ions is the magnetic dipole-magnetic dipole,

$W_{\text{md-md}}$, in Eq. (16) and (20). Thus, the selection rules are given by the $\left\langle \psi^* J^* \middle\| \hat{L} + g_S \hat{S} \middle\| \psi J \right\rangle$ matrix elements, which will be zero unless $\Delta J = 0, \pm 1$, except $J^* = J = 0$. As a result, the $W_{\text{md-md}}$ contribution to the ET rate *via* the Tb(Ⅲ) $^5D_4 \rightarrow {}^7F_5$ to Eu(Ⅲ) $^7F_0 \rightarrow {}^5D_1$ pathway will be nonzero because $\Delta J = \pm 1$ for both transitions, which satisfy the selection rules.

Notice that for Eu(Ⅲ), the first excited state $^7F_1$ is close to ground level $^7F_0$, so the populations of these states will depend on the temperature *via* the Boltzmann factor. When comparing the relative contributions of each mechanism to the total ET rate, it is common to weigh those rates involving the $^7F_0$ and $^7F_1$ levels by ca. 0.65 and 0.33 (at 300 K), respectively. However, care must be exercised when the ET rates are going to be employed in the rate equations. In this case, the thermal effects are already included in the initial populations when solving the rate equations, so the weighting procedure should not be overcounted.

7 Forced Electric Dipole Intensity Parameter, Ω_K(FED)

The forced electric dipole (FED) contribution to the intensity parameter Ω_K (with K =2, 4, and 6), that appears in the (forced) electric dipole strength S_d, Eq. (18), is perhaps one of the most difficult quantities to determine. It cannot be determined from fitted values of experimental absorption or emission spectra, because the fitted intensity parameters Ω_K contains contributions from both FED and dynamic coupling (DC) mechanisms. Usually, the FED contribution to Ω_K is very small; however, it depends on the lanthanide ion and its environment, so no trends have been observed[37,67-69]. It cannot be neglected, because despite it being small, the contributions of the $W_{\text{d-d}}$ and $W_{\text{dq-qd}}$ rates can be relevant or even dominant for several ET pathways. In addition, Ω_K(FED) contains effects from the environment of the lanthanide ion, which can be used to design systems with more efficient ET pathways. Therefore, values of Ω_K(FED) have to be obtained from quantitative models. For instance, the simple overlap model (SOM)[55,70] yields quantitative expressions for Ω_K(FED), which can be evaluated using the JOYSpectra web platform[71]. For Eu(Ⅲ) and Tb(Ⅲ) in a unique nine-coordination site of the doped material $Sr_3Tb_{0.90}Eu_{0.10}(PO_4)_3$[36,71], two sets of Ω_K(FED) $\{\Omega_2; \Omega_4; \Omega_6\}$ (in units of 10^{-20} cm^2) are obtained: {0.60; 0.21; 0.26} for Tb(Ⅲ) and {0.82; 0.38; 0.52} for Eu(Ⅲ).

These calculations were performed using the values of the force constant, $k_{Ln\text{-L}}$, of the *Ln*-Ligating atom bond obtained from density functional theory (DFT) calculations and, therefore, the values of the *g*-charge factors were determined for all *Ln*-O pairs with Eq. S80[36]. In the specific case of $Sr_3Tb_{0.90}Eu_{0.10}(PO_4)_3$ materials, the calculated $k_{\text{Ln-L}}$ is in the range of 0.38–0.42 mdyn/Å and it provides *g*-charge factors around 1.29. For further details on applying the SOM model, see Supporting Information and references [20, 35, 55, 67, 70-76].

8 Illustrative Examples of How to Calculate Energy Transfer Rates

Here we will illustrate step-by-step examples of some energy transfer pathways between *Ln*(Ⅲ) ions. The first example (**E1**) involves the Tb(Ⅲ)

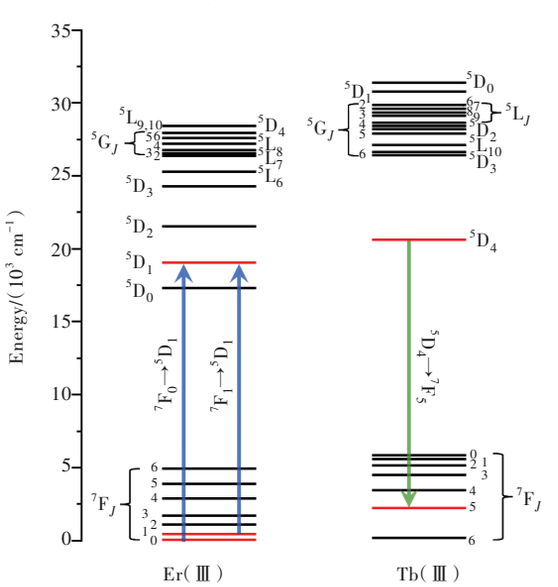

Fig.5 Energy level diagram showing Eu(Ⅲ) and Tb(Ⅲ) levels. The green arrow denotes the Tb(Ⅲ) $^5D_4 \rightarrow {}^7F_5$ transition (donor) while the blue lines represent Eu(Ⅲ) $^7F_{1,0} \rightarrow {}^5D_1$ transitions (acceptors). The levels involved in **E1** and **E2** are highlighted in red.

$[^5D_4 \rightarrow {}^7F_5]$ → Eu(Ⅲ) $[^7F_1 \rightarrow {}^5D_1]$ energy transfer pathway which is the dominant one for Tb-Eu processes[36-37]. As an exercise of a direct application of selection rules on J, the Tb(Ⅲ) $[^5D_4 \rightarrow {}^7F_5]$→Eu(Ⅲ) $[^7F_0 \rightarrow {}^5D_1]$ (**E2**) will also be addressed. These two pathways are illustrated in Fig. 5.

Since the discovery of the upconversion process by F. Auzel[77-78], ET between lanthanide ions has become an important issue regarding luminescent materials based on *Ln*(Ⅲ) ions[79-84]. Thus, we will also show how to calculate two energy transfer steps that are in good energy resonance conditions: Yb(Ⅲ) $[^2F_{5/2} \rightarrow {}^2F_{7/2}]$ → Er(Ⅲ) $[^4I_{15/2} \rightarrow {}^4I_{11/2}]$ (**E3**) and Yb(Ⅲ) $[^2F_{5/2} \rightarrow {}^2F_{7/2}]$ → Er(Ⅲ) $[^4I_{11/2} \rightarrow {}^4I_{7/2}]$ (**E4**) pathways[16,35]. Fig. 6 illustrates these pathways in **E3** and **E4**.

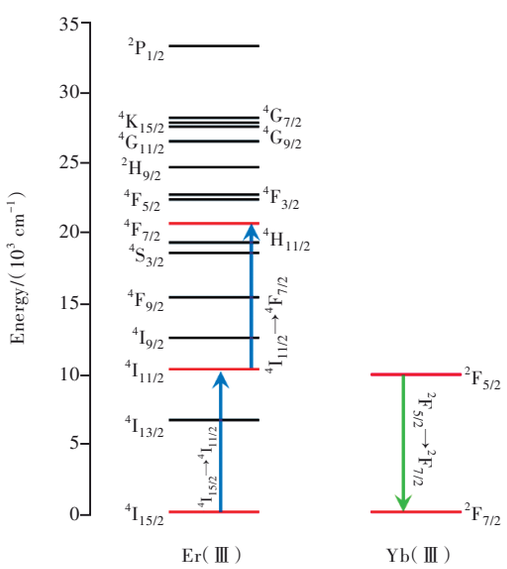

Fig.6　Energy level diagram showing Er(Ⅲ) and Yb(Ⅲ) levels. The green arrow denotes the Yb(Ⅲ) $^2F_{5/2} \rightarrow {}^2F_{7/2}$ transition (donor) while the blue lines represent the two upconverting transitions (acceptors) considered in **E3** and **E4**. All levels involved in the energy transfer examples are highlighted in red.

· E1

Tab. 1 contains the input data considering Tb(Ⅲ) $[^5D_4 \rightarrow {}^7F_5]$ and Eu(Ⅲ) $[^7F_1 \rightarrow {}^5D_1]$ transitions as donor and acceptor, respectively.

Thus, when the data in Tab. 1 is applied to the indicated equations with the sets of Ω_K(FED), mentioned previously for the case of $Sr_3Tb_{0.90}Eu_{0.10}(PO_4)_3$[36], we obtain the following rates for each mechanism:

Tab. 1　Input data used to calculate the Tb(Ⅲ) $[^5D_4 \rightarrow {}^7F_5]$ Eu(Ⅲ) $[^7F_1 \rightarrow {}^5D_1]$ in E1. The number of the equation where the input data enters is also indicated

	Eq.	Donor	Acceptor
J	18-20	4	1
ρ	21	0.057	0.057
$\langle \Vert U^{(2)} \Vert \rangle^2$	18-19	0.014 2	0.002 5
$\langle \Vert U^{(4)} \Vert \rangle^2$	18	0.001 3	0
$\langle \Vert U^{(6)} \Vert \rangle^2$	18	0.002 2	0
$\langle r^2 \rangle$ (10^{-17} cm^2)	19	2.30	2.57
$\langle \Vert L + 2S \Vert \rangle^2$	20	0.696	0.000 9
γ (cm^{-1})	23-24	350	350
	Eq.	Donor-Acceptor	
R_{DA}/cm	22	3.97×10^{-8}	
Δ/ cm^{-1}	23, 25	259	
ρ_{ff}	17	6.70×10^{-4} at 3.97 Å	

$$W_{d\text{-}d} = 6.6 \times 10^{-2}\ s^{-1},$$
$$W_{dq\text{-}qd} = 4.2 \times 10^{1}\ s^{-1},$$
$$W_{q\text{-}q} = 5.1 \times 10^{4}\ s^{-1},$$
$$W_{md\text{-}md} = 6.8 \times 10^{-1}\ s^{-1},$$
$$W_{ex} = 1.6 \times 10^{5}\ s^{-1}.$$

The total energy transfer rate is given by the sum of all these contributions and multiplied, in this case, by the $^7F_1$ population fraction (ca. 0.33 at room temperature):

$$W_{TOTAL} = 0.33 \times \left(W_{d\text{-}d} + W_{dq\text{-}qd} + W_{q\text{-}q} + W_{md\text{-}md} + W_{ex}\right) = 7.0 \times 10^{4}\ s^{-1}.$$

These rates are in agreement with those presented in reference[36] for the same pathway at the same R_{DA} distance. A slight deviation in the quadrupole-quadrupole mechanism from reference[36] ($W_{q\text{-}q} = 5.67 \times 10^{4}\ s^{-1}$) was observed. This is due to the use of $\langle r^2 \rangle = 2.57 \times 10^{-17}$ for the Tb(Ⅲ).

· E2

To estimate each contribution to the rate of the Tb(Ⅲ) $[^5D_4 \rightarrow {}^7F_5]$ → Eu(Ⅲ) $[^7F_0 \rightarrow {}^5D_1]$ pathway, some values in Tab. 1 need to be updated to match the $^7F_0 \rightarrow {}^5D_1$ transition (Tab. 2).

It can be noticed that for this pathway, according to the selection rules, the $^7F_0 \rightarrow {}^5D_1$ transition has all $\langle \Vert U^{(K)} \Vert \rangle^2 = 0$. Therefore, $W_{d\text{-}d} = W_{dq\text{-}qd} = W_{q\text{-}q} = 0$ and this pathway has only the contributions of the $W_{ex} = 3.3 \times 10^{3}\ s^{-1}$ and $W_{md\text{-}md} = 1.3 \times 10^{1}\ s^{-1}$,

Tab. 2 Input data used to calculate the Tb(Ⅲ) [$^5D_4 \rightarrow {}^7F_5$] → Eu(Ⅲ) [$^7F_0 \rightarrow {}^5D_1$] in E2. The number of the equation where the input data enters is also indicated. The other quantities that are not displayed are still the same as presented in Tab. 1

	Eq.	Donor	Acceptor
J	18-20	4	0
$\langle \|U^{(2)}\| \rangle^2$	18-19	0.014 2	0
$\langle \|U^{(4)}\| \rangle^2$	18	0.001 3	0
$\langle \|U^{(6)}\| \rangle^2$	18	0.002 2	0
$\langle \|L + 2S\| \rangle^2$	20	0.696	0.027 3
γ (cm^{-1})	23-24	350	106
	Eq.	Donor-Acceptor	
Δ /cm^{-1}	23, 25	−631	

in accordance with those in reference[36]. Adding these rates, considering the $^7F_0$ population fraction (ca. 0.64 at room temperature), and the energy barrier factor $G(\Delta,T)$, yields the total rate:

$$W_{TOTAL} = 0.64 \times G(\Delta, T) \times (W_{md\text{-}md} + W_{ex}) = 1.0 \times 10^3\ s^{-1}.$$

It is important to pay attention that, in this case, $G(\Delta, T)$ was considered outside of the F-factor just to match with the data in the literature. But it must be considered for each case appropriately.

· E3

The first step in the Yb-Er upconversion process is given by the Yb(Ⅲ)[$^2F_{5/2} \rightarrow {}^2F_{7/2}$] → Er(Ⅲ) [$^4I_{15/2} \rightarrow {}^4I_{11/2}$] pathway. Tab. 3 contains the data for calculating the pairwise energy transfer for the shorter Yb-Er distance (R_{DA} = 3.5 Å) in $NaYF_4$: Yb,Er material.

Applying the data in Tab. 3 leads to:

$$W_{d\text{-}d} = 5.2 \times 10^2\ s^{-1},$$
$$W_{dq\text{-}qd} = 3.1 \times 10^4\ s^{-1},$$
$$W_{q\text{-}q} = 3.2 \times 10^6\ s^{-1},$$
$$W_{md\text{-}md} = 0,$$
$$W_{ex} = 3.6 \times 10^6\ s^{-1}.$$

The total pairwise energy transfer Yb(Ⅲ) [$^2F_{5/2} \rightarrow {}^2F_{7/2}$] → Er(Ⅲ) [$^4I_{15/2} \rightarrow {}^4I_{11/2}$] pathway is $W_{TOTAL} = 6.9 \times 10^6\ s^{-1}$, which also reproduces the value for the shortest Yb-Er distance for the first upconverting step from reference[16].

Tab. 3 Input data used to calculate Yb(Ⅲ) [$^2F_{5/2} \rightarrow {}^2F_{7/2}$] → Er(Ⅲ) [$^4I_{15/2} \rightarrow {}^4I_{11/2}$] in E3. The number of the equation where the input data enters is also indicated. The values of Ω_K represent those obtained only with the FED contribution

	Eq.	Donor	Acceptor
J	18-20	5/2	15/2
ρ	21	0.065	0.065
$\langle \|U^{(2)}\| \rangle^2$	18-19	0.122 5	0.027 6
$\langle \|U^{(4)}\| \rangle^2$	18	0.409 6	0.000 2
$\langle \|U^{(6)}\| \rangle^2$	18	0.857 5	0.394 2
Ω_2 (10^{-20} cm^2)	18	0.067	0.065
Ω_4 (10^{-20} cm^2)	18	0.229	0.259
Ω_6 (10^{-20} cm^2)	18	0.551	0.637
$\langle r^2 \rangle$ (10^{-17} cm^2)	19	1.82	1.99
$\langle \|L + 2S\| \rangle^2$	20	30.86	0
γ (cm^{-1})	23-24	400	450
	Eq.	Donor-Acceptor	
R_{DA} /cm	22	3.50×10^{-8}	
Δ /cm^{-1}	23, 25	129	
ρ_{ff}	17	1.38×10^{-3} at 3.50 Å	

· E4

Repeating the same procedure as **E3** but updating the acceptor transition from $^4I_{15/2} \rightarrow {}^4I_{11/2}$ to $^4I_{11/2} \rightarrow {}^4I_{7/2}$, we obtain the input data in Tab. 4.

Tab. 4 Input data used to calculate the Yb(Ⅲ) [$^2F_{5/2} \rightarrow {}^2F_{7/2}$] → Er(Ⅲ) [$^4I_{11/2} \rightarrow {}^4I_{7/2}$] in E4. The number of the equation where the input data enters is also indicated

	Eq.	Donor	Acceptor
J	18-20	5/2	11/2
$\langle \|U^{(2)}\| \rangle^2$	18-19	0.122 5	0.032 0
$\langle \|U^{(4)}\| \rangle^2$	18	0.409 6	0.265 3
$\langle \|U^{(6)}\| \rangle^2$	18	0.857 5	0.154 5
$\langle \|L + 2S\| \rangle^2$	20	30.86	0
	Eq.	Donor-Acceptor	
Δ/cm^{-1}	23, 25	−111	

In this case, the total pairwise energy transfer of the Yb(Ⅲ) [$^2F_{5/2} \rightarrow {}^2F_{7/2}$] → Er(Ⅲ) [$^4I_{11/2} \rightarrow {}^4I_{7/2}$] pathway is $W_{TOTAL} = 5.1 \times 10^6\ s^{-1}$, in agreement with the value for the shortest Yb-Er distance for the second upconverting step from reference[16].

All these examples are worked out as separated Mathcad® script files available in the Supporting Information (Examples_Mathcad.zip).

9 Conclusions

In this tutorial review, we presented the equations for the energy transfer rates between lanthanide ions in an alternative form, which aimed at an easier interpretation and a simpler step-by-step calculation. Four examples were provided to illustrate this procedure for relevant lanthanide pairs. We expect that the present work will guide students and stimulate the research fn the field of energy transfer between lanthanide ions.

Acknowledgments

The authors are grateful for the financial support from CNPq, CAPES, FACEPE, and FINEP agencies. This work was funded by the Public Call n. 03 Produtividade em Pesquisa PROPESQ/PRPG/UFPB project number PVN13305-2020, and PROPESQ/CNPq/UFPB PIN11132-2019. This work was developed within the scope of the project CICECO-Aveiro Institute of Materials, UIDB/50011/2020 and UIDP/50011/2020, financed by Portuguese funds through the FCT/MEC and when appropriate co-financed by FEDER under the PT2020 Partnership Agreement. RLL is grateful for the partial financial support under grants: Pronex APQ-0675-1.06/14, INCT-NANOMARCS APQ-0549-1.06/17, APQ-1007-1.06/15, and CNPq-PQ fellowship (Proc. 309177/2018-9).

Author Statement

Albano N. Carneiro Neto: Conceptualization, Methodology, Software, Validation, Formal analysis, Investigation, Data Curation, Writing-Original Draft, Writing-Review & Editing. Renaldo T. Moura Jr.: Conceptualization, Writing-Review & Editing. Jorge A. A. Coelho: Conceptualization, Methodology, Writing-Review & Editing. Mauro E. Silva-Junior: Conceptualization, Writing-Review & Editing. Janderson L. Costa: Conceptualization, Writing-Review & Editing. Oscar L. Malta: Conceptualization, Methodology, Formal analysis, Writing-Original Draft, Writing-Review & Editing, Supervision. Ricardo L. Longo: Conceptualization, Methodology, Investigation, Formal analysis, Writing-Original Draft, Writing-Review & Editing, Validation, Supervision, Project administration.

Supplementary Information and Response Letter are available for this paper at: http://cjl.lightpublishing.cn/thesisDetails#10.37188/CJL.EN20220007.

References:

[1] JAHNKE T, SANN H, HAVERMEIER T, *et al.* Ultrafast energy transfer between water molecules [J]. *Nat. Phys.*, 2010, 6(2): 139-142.

[2] XUAN M J, ZHAO J, SHAO J X, *et al.* Perspective of energy transfer from light energy into biological energy [J]. *Green Energy Environ.*, 2017, 2(1): 18-22.

[3] XU W L, BONY B A, KIM C R, *et al.* Mixed lanthanide oxide nanoparticles as dual imaging agent in biomedicine [J]. *Sci. Rep.*, 2013, 3: 3210-1-10.

[4] WIESZCZYCKA K, STASZAK K, WOŹNIAK-BUDYCH M J, *et al.* Lanthanides and tissue engineering strategies for bone regeneration [J]. *Coord. Chem. Rev.*, 2019, 388: 248-267.

[5] ZHANG Y, WEI W, DAS G K, *et al.* Engineering lanthanide-based materials for nanomedicine [J]. *J. Photochem. Photobiol. C: Photochem. Rev.*, 2014, 20: 71-96.

[6] RAMALHO J F C B, DIAS L M S, FU L S, *et al.* Customized luminescent multiplexed quick-response codes as reliable temperature mobile optical sensors for ehealth and internet of things [J]. *Adv. Photonics Res.*, 2022, 3(6): 2100206-1-11.

[7] DE CARVALHO M A, TALHAVINI M, PIMENTEL M F, *et al.* NIR hyperspectral images for identification of gunshot residue from tagged ammunition [J]. *Anal. Methods*, 2018, 10(38): 4711-4717.

[8] ZHOU B, YAN L, HUANG J S, *et al.* NIR II-responsive photon upconversion through energy migration in an ytterbium sublattice [J]. *Nat. Photonics*, 2020, 14(12): 760-766.

[9] FAN J Y, LIANG L L, GU Y Y, *et al*. (INVITED) Opposing effects of energy migration and cross-relaxation on surface sensitivity of lanthanide-doped nanocrystals [J]. *Opt. Mater.* X, 2021, 12: 100104.

[10] BETTINELLI M, CARLOS L, LIU X G. Lanthanide-doped upconversion nanoparticles [J]. *Phys. Today*, 2015, 68(9): 38-44.

[11] STREK W. Concentration dependence of the phonon-assisted energy transfer between rare-earth ions [J]. *Phys. Rev.* B, 1984, 29(12): 6957-6962.

[12] AUZEL F. History of upconversion discovery and its evolution [J]. *J. Lumin.*, 2020, 223: 116900-1-7.

[13] AUZEL F. Upconversion and anti-Stokes processes with f and d ions in solids [J]. *Chem. Rev.*, 2004, 104(1): 139-174.

[14] DONG H, SUN L D, YAN C H. Energy transfer in lanthanide upconversion studies for extended optical applications [J]. *Chem. Soc. Rev.*, 2015, 44(6): 1608-1634.

[15] NONAT A, LIU T, JEANNIN O, *et al*. Energy transfer in supramolecular heteronuclear lanthanide dimers and application to fluoride sensing in water [J]. *Chem. -A Eur. J.*, 2018, 24(15): 3784-3792.

[16] QIN X, NETO A N C, LONGO R L, *et al*. Surface plasmon-photon coupling in lanthanide-doped nanoparticles [J]. *J. Phys. Chem. Lett.*, 2021, 12(5): 1520-1541.

[17] ZOU K S, GUO H T, LU M, *et al*. Broad-spectrum and long-lifetime emissions of Nd^{3+} ions in lead fluorosilicate glass [J]. *Opt. Express*, 2009, 17(12): 10001-10009.

[18] IRFANULLAH M, IFTIKHAR K. The correlation between *f-f* absorption and sensitized visible light emission of luminescent Pr(Ⅲ) complexes: role of solvents and ancillary ligands on sensitivity [J]. *J. Fluoresc.*, 2011, 21(2): 673-686.

[19] HATANAKA M, YABUSHITA S. Theoretical study on the *f-f* transition intensities of lanthanide trihalide systems [J]. *J. Phys. Chem.* A, 2009, 113(5): 12615-12625.

[20] NETO A N C, TEOTONIO E E S, DE SÁ G F, *et al*. Modeling intramolecular energy transfer in lanthanide chelates: a critical review and recent advances [J]. *Handb. Phys. Chem. Rare Earths*, 2019, 56: 55-162.

[21] SCHATZ G C, RATNER M A. *Quantum Mechanics in Chemistry* [M]. Mineola: Dover Publications, Inc., 2002.

[22] ATKINS P, FRIEDMAN R. *Molecular Quantum Mechanics* [M]. New York: Oxford University Press, 2005.

[23] JUDD B R. *Operator Techniques in Atomic Spectroscopy* [M]. Princeton: Princeton University Press, 1998.

[24] FORSTER T. Energiewanderung und fluoreszenz [J]. *Naturwissenschaften*, 1946, 33(6): 166-175.

[25] DEXTER D L. A theory of sensitized luminescence in solids [J]. *J. Chem. Phys.*, 1953, 21(5): 836-850.

[26] NASIRI S, BUBIN S, ADAMOWICZ L. Treating the motion of nuclei and electrons in atomic and molecular quantum mechanical calculations on an equal footing: non-Born-Oppenheimer quantum chemistry [M]. RUUD K, BRÄNDAS E J. *Chemical Physics and Quantum Chemistry*. Cambridge, Massachusetts: Academic Press Inc., 2020: 143-166.

[27] WOOLLEY R G, SUTCLIFFE B T. Molecular structure and the Born-Oppenheimer approximation [J]. *Chem. Phys. Lett.*, 1977, 45(2): 393-398.

[28] PRAVEEN V K, RANJITH C, BANDINI E, *et al*. Oligo(phenylenevinylene) hybrids and self-assemblies: versatile materials for excitation energy transfer [J]. *Chem. Soc. Rev.*, 2014, 43(12): 4222-4242.

[29] OH J M, VENTERS C C, DI C, *et al*. U1 snRNP regulates cancer cell migration and invasion in vitro [J]. *Nat. Commun.*, 2020, 11(1): 1-1-8.

[30] KASPRZYCKA E, NETO A N C, TRUSH V A, *et al*. [J]. *Spectrochim. Acta Part* A: *Mol. Biomol. Spectrosc.*, 2022: 121072.

[31] LYUBOV D M, NETO A N, FAYOUMI A, *et al*. Employing three-blade propeller lanthanide complexes as molecular luminescent thermometers: study of temperature sensing through a concerted experimental/theory approach [J]. *J. Mater. Chem.* C, 2022, 10(18): 7176-7188.

[32] MALTA O L. Ligand—rare-earth ion energy transfer in coordination compounds. A theoretical approach [J]. *J. Lumin.*, 1997, 71(3): 229-236.

[33] MALTA O L, SILVA F R G E, LONGO R. On the dependence of the luminescence intensity of rare-earth compounds with pressure: a theoretical study of $Eu(TTF)_3 2H_2O$ in polymeric solution and crystalline phases [J]. *Chem. Phys. Lett.*, 1999, 307(5-6): 518-526.

[34] MALTA O L. Mechanisms of non-radiative energy transfer involving lanthanide ions revisited [J]. *J. Non. -Cryst. Solids*,

2008, 354(42-44): 4770-4776.

[35] NETO A N C, MOURA R T J R, MALTA O L. On the mechanisms of non-radiative energy transfer between lanthanide ions: centrosymmetric systems [J]. *J. Lumin.*, 2019, 210: 342-347.

[36] NETO A N C, MOURA R T J R, SHYICHUK A, *et al.* Theoretical and experimental investigation of the $Tb^{3+} \rightarrow Eu^{3+}$ energy transfer mechanisms in cubic $A_3Tb_{0.90}Eu_{0.10}(PO_4)_3$ (A = Sr, Ba) materials [J]. *J. Phys. Chem.* C, 2020, 124(18): 10105-10116.

[37] TRANNOY V, NETO A N C, BRITES C D S, *et al.* Engineering of mixed Eu^{3+}/Tb^{3+} metal-organic frameworks luminescent thermometers with tunable sensitivity [J]. *Adv. Opt. Mater.*, 2021, 9(6): 2001938-1-12.

[38] KUSHIDA T. Energy transfer and cooperative optical transitions in rare-earth doped inorganic materials. I. transition probability calculation [J]. *J. Phys. Soc. Japan*, 1973, 34(5): 1318-1326.

[39] JUDD B R. Optical absorption intensities of rare-earth ions [J]. *Phys. Rev.*, 1962, 127(3): 750-761.

[40] OFELT G S. Intensities of crystal spectra of rare-earth ions [J]. *J. Chem. Phys.*, 1962, 37(3): 511-520.

[41] MALTA O L, SILVA F R G E. A theoretical approach to intramolecular energy transfer and emission quantum yields in coordination compounds of rare earth ions [J]. *Spectrochim. Acta Part* A: *Mol. Biomol. Spectrosc.*, 1998, 54(11): 1593-1599.

[42] FANO U, RACAH G. *Irreducible Tensorial Sets* [M]. New York: Academic Press Inc., 1959.

[43] NETO A N C, MAMONTOVA E, BOTAS A M P, *et al.* Rationalizing the thermal response of dual-center molecular thermometers: the example of an Eu/Tb coordination complex [J]. *Adv. Opt. Mater.*, 2022, 10(5): 2101870.

[44] CODATA Value: electron g factor. The NIST reference on constants, units, and uncertainty [EB/OL]. [2022-06-19]. https://physics.nist.gov/cgi-bin/cuu/Value?gem.

[45] BINNEMANS K. Interpretation of europium(Ⅲ) spectra [J]. *Coord. Chem. Rev.*, 2015, 295: 1-45.

[46] CARNALL W T, FIELDS P R, RAJNAK K. Electronic energy levels in the trivalent lanthanide aquo ions. I. Pr^{3+}, Nd^{3+}, Pm^{3+}, Sm^{3+}, Dy^{3+}, Ho^{3+}, Er^{3+}, and Tm^{3+} [J]. *J. Chem. Phys.*, 1968, 49(10): 4424-4442.

[47] CARNALL W T, CROSSWHITE H, CROSSWHITE H M. *Energy Level Structure and Transition Probabilities in the Spectra of the Trivalent Lanthanides in* LaF_3 [R]. Argonne: Argonne National Lab, 1978.

[48] OFELT G S. Structure of the f^6 configuration with application to rare-earth ions [J]. *J. Chem. Phys.*, 1963, 38(9): 2171-2180.

[49] RAJNAK K. Configuration-interaction effects on the "free-ion" energy levels of Nd^{3+} and Er^{3+} [J]. *J. Chem. Phys.*, 1965, 43(5): 847-855.

[50] WYBOURNE B G. Structure of f^n configurations. II. f^5 and f^9 configurations [J]. *J. Chem. Phys.*, 1962, 36(9): 2301-2311.

[51] NETO A N C, KASPRZYCKA E, SOUZA A S, *et al.* On the long decay time of the $^7F_5$ level of Tb^{3+} [J]. *J. Lumin.*, 2022, 248: 118933.

[52] EDVARDSSON S, KLINTENBERG M. Role of the electrostatic model in calculating rare-earth crystal-field parameters [J] *J. Alloys Compd.*, 1998, 275-277: 230-233.

[53] NETO A N C, MOURA R T JR. Overlap integrals and excitation energies calculations in trivalent lanthanides 4*f* orbitals in pairs *Ln-L* (*L* = *Ln*, N, O, F, P, S, Cl, Se, Br, and I) [J]. *Chem. Phys. Lett.*, 2020, 757: 137884-1-6.

[54] MALTA O L, BRITO H F, MENEZES J F S, *et al.* Spectroscopic properties of a new light-converting device Eu(thenoyltrifluoroacetonate)$_3$ 2(dibenzyl sulfoxide). A theoretical analysis based on structural data obtained from a sparkle model [J]. *J. Lumin.*, 1997, 75(3): 255-268.

[55] MALTA O L. Theoretical crystal-field parameters for the YOCl: Eu^{3+} system. A simple overlap model [J]. *Chem. Phys. Lett.*, 1982, 88(3): 353-356.

[56] PATERLINI V, PICCINELLI F, BETTINELLI M. $Tb^{3+} \rightarrow Eu^{3+}$ energy transfer processes in eulytite $A_3Tb(PO_4)_3$ (A=Sr, Ba) and silico-carnotite $Ca_3Tb_2Z_3O_{12}$ (Z=Si, Ge) materials doped with Eu^{3+} [J]. *Phys.* B: *Condens. Matter*, 2019, 575: 411685-1-5.

[57] TANNER P A, CHUA M, REID M F. Energy transfer by magnetic dipole-magnetic dipole interaction [J]. *Chem. Phys. Lett.*, 1993, 209(5-6): 539-546.

[58] CHUA M, TANNER P A, REID M F. Energy transfer by electric dipole-magnetic dipole interaction in cubic crystals

[J]. *Solid State Commun.*, 1994, 90(9): 581-583.

[59] MALTA O L. Energy transfer between molecules and small metallic particles [J]. *Phys. Lett.* A, 1986, 114(4): 195-197.

[60] SMENTEK L, KĘDZIORSKI A. Efficiency of the energy transfer in lanthanide-organic chelates; spectral overlap integral [J]. *J. Lumin.*, 2010, 130(7): 1154-1159.

[61] BECKE A D. Density-functional exchange-energy approximation with correct asymptotic behavior [J]. *Phys. Rev.* A, 1988, 38(6): 3098-3100.

[62] PERDEW J P. Density-functional approximation for the correlation energy of the inhomogeneous electron gas [J]. *Phys. Rev.* B, 1986, 33(12): 8822-8824.

[63] VAN LENTHE E, BAERENDS E J. Optimized Slater-type basis sets for the elements 1-118 [J]. *J. Comput. Chem.*, 2003, 24(9): 1142-1156.

[64] VAN LENTHE E, SNIJDERS J G, BAERENDS E J. The zero-order regular approximation for relativistic effects: the effect of spin-orbit coupling in closed shell molecules [J]. *J. Chem. Phys.*, 1996, 105(15): 6505-6516.

[65] VAN LENTHE E, EHLERS A, BAERENDS E J. Geometry optimizations in the zero order regular approximation for relativistic effects [J]. *J. Chem. Phys.*, 1999, 110(18): 8943-8953.

[66] VELDE GTE, BICKELHAUPT F M, BAERENDS E J, *et al*. Chemistry with ADF [J]. *J. Comput. Chem.*, 2001, 22(9): 931-967.

[67] MOURA R T JR, NETO A N C, LONGO R L, *et al*. On the calculation and interpretation of covalency in the intensity parameters of 4f-4f transitions in Eu^{3+} complexes based on the chemical bond overlap polarizability [J]. *J. Lumin.*, 2016, 170: 420-430.

[68] AQUINO L EDO N, BARBOSA G A, DE L RAMOS J, *et al*. Seven-coordinate Tb^{3+} complexes with 90% quantum yields: high-performance examples of combined singlet- and triplet-to-Tb^{3+} energy-transfer pathways [J]. *Inorg. Chem.*, 2021, 60(2): 892-907.

[69] MOURA R T JR, OLIVEIRA J A, SANTOS I A, *et al*. Theoretical evidence of the singlet predominance in the intramolecular energy transfer in ruhemann's purple Tb(Ⅲ) complexes [J]. *Adv. Theory Simul.*, 2021, 4(3): 2000304-1-10.

[70] MALTA O L. A simple overlap model in lanthanide crystal-field theory [J]. *Chem. Phys. Lett.*, 1982, 87(1): 27-29.

[71] MOURA R T JR, NETO A N C, AGUIAR E C, *et al*. (INVITED) JOYSpectra: A web platform for luminescence of lanthanides [J]. *Opt. Mater.* X, 2021, 11: 100080.

[72] ASSUNÇÃO I P, NETO A N C, MOURA R T JR, *et al*. Odd-even effect on luminescence properties of europium aliphatic dicarboxylate complexes [J]. *ChemPhysChem*, 2019, 20(15): 1931-1940.

[73] SHYICHUK A, MOURA R T JR, NETO A N C, *et al*. Effects of dopant addition on lattice and luminescence intensity parameters of Eu(Ⅲ)-doped lanthanum orthovanadate [J]. *J. Phys. Chem.* C, 2016, 120(50): 28497-28508.

[74] GRZYB T, SZCZESZAK A, SHYICHUK A, *et al*. Comparative studies of structure, spectroscopic properties and intensity parameters of tetragonal rare earth vanadate nanophosphors doped with Eu(Ⅲ) [J]. *J. Alloys Compd.*, 2018, 741: 459-472.

[75] SHYICHUK A, CÂMARA S S, WEBER I T, *et al*. Energy transfer upconversion dynamics in YVO_4: Yb^{3+}, Er^{3+} [J]. *J. Lumin.*, 2016, 170: 560-570.

[76] NETO A N C, MOURA R T JR, AGUIAR E C, *et al*. Theoretical study of geometric and spectroscopic properties of Eu(Ⅲ) complexes with Ruhemann's Purple ligands [J]. *J. Lumin.*, 2018, 201: 451-459.

[77] AUZEL F. Compteur quantique par transfert denergie de Yb^{3+} a Tm^{3+} dans un tungstate mixte et dans un verre germanate [J]. *Acad. des Sci. Ser.* B, 1966, 263: 819.

[78] AUZEL F. Upconversion processes in coupled ion systems [J]. *J. Lumin.*, 1990, 45(1-6): 341-345.

[79] YE Y S, JIANG Z H, WANG Q Z, *et al*. Upconversion luminescence of $NaYF_4$: Yb, Er nanocrystals with high uniformity [J]. *J. Rare Earths*, 2014, 32(9): 802-805.

[80] SUN Y J, CHEN Y, TIAN L J, *et al*. Controlled synthesis and morphology dependent upconversion luminescence of $NaYF_4$: Yb, Er nanocrystals [J]. *Nanotechnology*, 2007, 18(27): 275609-1-9.

[81] LIU M, SHI Z Y, WANG X, *et al*. Simultaneous enhancement of red upconversion luminescence and CT contrast of $NaGdF_4$: Yb, Er nanoparticles *via* Lu^{3+} doping [J]. *Nanoscale*, 2018, 10(43): 20279-20288.

[82] LI L, LIN H H, ZHAO X Q, *et al.* Effect of Yb^{3+} concentration on upconversion luminescence in Yb^{3+}, Tm^{3+} co-doped Lu_2O_3 nanophosphors [J]. *J. Alloys Compd.*, 2014, 586: 555-560.

[83] LIANG L L, TEH D B L, DINH N D, *et al.* Upconversion amplification through dielectric superlensing modulation [J]. *Nat. Commun.*, 2019, 10(1): 1391.

[84] TU L P, LIU X M, WU F, *et al.* Excitation energy migration dynamics in upconversion nanomaterials [J]. *Chem. Soc. Rev.*, 2015, 44(6): 1331-1345.

Albano N. Carneiro Neto(1985–), received his Ph. D. in Chemistry from Federal University of Pernambuco (Brazil) in 2018, started as a pos-doc from 2019 to 2021 at University of Aveiro (Portugal) and nowadays he is a Researcher at the Physics Department and CICECO-Aveiro Institute of Materials, University of Aveiro. He acted as guest editor of *Journal of Luminescence* in 2018 and he is a member of the topical advisory panel of *Applied Sciences*. His scientific interests are lanthanides chemistry; quantum chemistry calculations; covalency and chemical bonding; thermometry; f-f intensities; Judd-Ofelt theory; ligand- and lanthanide-to-lanthanide energy transfer. He authored 47 papers in international journals and 04 book chapters. According to Google Scholar (November 2022), he has more than 920 citations with an h-index of 18.

E-mail: albanoneto@ua. pt

Oscar L. Malta(1954–), Ph. D. at Université Pierre et Marie Curie-Paris 6 (France, 1981). He is a Full Professor in the Department of Fundamental Chemistry of the UFPE (Brazil), researcher 1A of the National Council of Scientific and Technological Development, and member of the Brazilian Academy of Science. He was awarded the Prof. Ricardo Ferreira Award for Scientific Merit (granted by Pernambuco State Foundation for Science and Technology) and the Prof. Paulo Duarte medal (granted by The Brazilian Association of Chemistry). Received the medal of the National Order of the Scientific Merit (Brazilian Government, 2018). He had a Special Issue in the *Journal of Luminescence* dedicated to his 60s. He was the Chairman of the 18th International Conference on Luminescence, ICL-2017. He is Doctor Honoris Causa by the University of Wrocław. His research interests are in Chemistry and Physics, with emphasis on atomic and molecular spectroscopy, compounds with lanthanide ions, and nanostructured materials.

E-mail: oscar. malta@ufpe. br

Ricardo L. Longo(1964–), Ph. D. from University of Florida (USA, 1993) and pos-doc at the Quantum Theory Project (U. of Florida). Since 1994 he is a professor at the Department of Fundamental Chemistry, Federal University at Pernambuco, Recife, Brazil. He was a visiting at McGill University, Montrèal, Canada (2016) and visiting consultant at University of Aveiro, Portugal (2019). Served as associate editor of *Journal of the Brazilian Chemical Society* (2006–2012) and guest editor of *Journal of Luminescence* (2016 and 2018). He is an advisor/reviewer in Brazilian funding agencies (CAPES, FACEPE). His scientific interests cover the development of theoretical and computational methods to physical chemistry, particularly to molecular spectroscopy, thermometry, chemical reactions, hydrogen bonded systems and complex networks. Supervised 10 post-docs, 22 Ph. D., 21 MSc, and 26 undergraduate students in the Chemistry and Materials Science Programs. Currently, he is supervising 08 Ph. D. and 04 MSc students. He authored 04 book chapters and about 110 papers.

E-mail: ricardo. longo@ufpe. br